International Journal of Mass Spectrometry 311 (2012) 7–16

Contents lists available at SciVerse ScienceDirect

International Journal of Mass Spectrometry

journal homepage: www.elsevier.com/locate/ijms

Mass spectrometry of anions and cations produced in 1–4 keV H^-, O^-, and OH^- collisions with nitromethane, water, ethanol, and methanol

D. Almeida [a], R. Antunes [a], G. Martins [a], G. Garcia [b,c], R.W. McCullough [d], S. Eden [e,f,*], P. Limão-Vieira [a,e,**]

[a] Laboratório de Colisões Atómicas e Moleculares, CEFITEC, Departamento de Física, FCT – Universidade Nova de Lisboa, P-2829-516 Caparica, Portugal
[b] Departamento de Física de los Materiales, UNED, Senda del Rey 9, 28040 Madrid, Spain
[c] Instituto de Física Fundamental, Consejo Superior de Investigaciones Científicas, Serrano 113-bis, 28006 Madrid, Spain
[d] Queens University Belfast, School of Mathematics & Physics, Centre for Plasma Physics, Belfast BT7 1NN, Co. Antrim North Ireland, UK
[e] Department of Physical Sciences, Open University, Walton Hall, Milton Keynes MK7 6AA, UK
[f] Institut de Physique Nucléaire de Lyon, IN2P3-CNRS et Université Claude Bernard Lyon 1, 43, boulevard du 11 Novembre 1918, 69622 Villeurbanne Cedex, France

ARTICLE INFO

Article history:
Received 13 October 2011
Received in revised form
17 November 2011
Accepted 17 November 2011
Available online 17 December 2011

Keywords:
Negative and positive ion formation
Dipole-bound state

ABSTRACT

Interactions between 1 and 4 keV anions (H^-, O^-, and OH^-) and gas-phase molecules (nitromethane, water, ethanol, and methanol) have been studied using quadrupole mass spectrometry of the product anions and cations. The low collision velocities (0.07–0.40 v_{Bohr}) provide favourable conditions for electron transfer from the anion projectile to the neutral target molecule yielding negative ion formation, while strong competition with cation formation is also observed. Relative production of fragment cations increases with H^- impact energy and with projectile mass when energy is constant. Considered together, these results suggest a momentum dependence on collisional energy deposition. As far as negative ion production is concerned, comparisons with previous free electron attachment studies are drawn as a starting point for the interpretation of the anion fragmentation channels. For nitromethane and water, the present anion fragmentation patterns are substantially different to the free electron attachment data. Conversely the fragmentation channels of ethanol and methanol anions only show clear dependence on the electron attachment/transfer process in terms of the relative anion yields.

1. Introduction

The importance of negative ion chemistry in the upper atmosphere is of recent interest amongst the astrochemistry community. It is now well established that negative ions exist in the upper atmosphere of Titan [1], produced by mechanisms such as three-body (dissociative) electron attachment. Indeed, Titan's upper atmosphere is composed of several types of organic molecules, which are believed to be the building blocks of other, more complicated, biological molecules (Ref. [1] and references therein). As such, the study of anion collisions with simple organic molecules may provide some insight to the negative ion chemistry in relevant atmospheric systems. Some of the molecules studied herein (water, methanol and ethanol) are some of the more fundamental organic molecules and as such, their study may provide some insight on interactions of other more complex astrochemically relevant organic molecules. Furthermore, within the scope of astrochemistry, the study of anion collisions with H^-, O^- and OH^- as projectiles is quite critical since it is known that these anions are quite abundant in the upper earth's atmosphere, albeit at much lower (thermal) energies. Still, the difference in projectile's kinetic energy between our study and the astrophysical environment does not detract from the value of this work since the fundamental mechanisms surrounding both systems will mostly be the same.

From a more fundamental point of view, the potential role of the neutral atom as a stabilizing third body *post* electron transfer from the incident anion is of particular interest. Despite the fact that the collision energies of the projectiles in this study are far above the ones in alkali atom–molecule collisions, comparisons with the latter [2–4], and also with free electron attachment experiments can enhance our understanding of such stabilization effects on the mass spectrum of anions due to the target molecule. Regardless of the electron capture mechanism, electron transfer from the projectile to the acceptor molecule results in a transient negative ion (TNI), which can decay via electron auto-detachment or fragmentation of the anion. As far as we are aware, no previous experimental or theoretical studies pertaining to the fragmentation patterns in collisions with anion projectiles have been carried out in the present

* Corresponding author at: Department of Physical Sciences, Open University, Walton Hall, Milton Keynes MK7 6AA, UK.
** Corresponding author at: Departamento de Física, FCT – Universidade Nova de Lisboa 2829-516, Portugal. Tel.: +351 212948576; fax: +351 212948549.
E-mail addresses: s.p.eden@open.ac.uk (S. Eden), plimaovieira@fct.unl.pt (P. Limão-Vieira).

1387-3806/$ – see front matter © 2011 Elsevier B.V. All rights reserved.
doi:10.1016/j.ijms.2011.11.009

Table 1
Summary of anion–molecule collisions studied using product cation mass spectrometry.

Ion	Binding energy of attached electron (eV) [11]	Ionization energy of neutral (eV) [11]	Kinetic energy (keV)	Anion velocity (v_{Bohr})	Target molecules
H^-	0.75	13.60	1	0.20	CH_3NO_2
			2	0.28	CH_3NO_2, H_2O
			4	0.40	CH_3NO_2, H_2O, CH_3OH, C_2H_5OH
O^-	1.46	13.62	2	0.07	H_2O
			4	0.10	CH_3NO_2, H_2O, CH_3OH, C_2H_5OH
OH^-	1.92	13.02	2	0.07	H_2O
			4	0.10	CH_3NO_2, H_2O, CH_3OH, C_2H_5OH

range (0.07–0.40 v_{Bohr}). Moreover, the present work provides the first data for anion (or indeed cation) production in anion collisions with molecules of greater complexity than N_2 and H_2. Most of the literature regarding anion–molecule collisions at a velocity range of $0.1 < v/v_{Bohr} < 0.4$ pertains to the study of electron detachment post-collision [5–9]. Two main mechanisms are responsible for this; direct detachment (DD) and charge transfer to shape resonance (CTSR). The first process involves electron detachment from the collision complex without any formation of a temporary negative ion (TNI), for example:

$$X^- + AB \rightarrow X + AB + e^- \quad DD$$

where X^- represents the anion projectile and AB represents a molecular target. The second process involves charge transfer of the electron from the anion to the molecule, thereby creating a short-lived TNI. Due to the low lifetimes of the TNI, the electron is subsequently ejected.

$$X^- + AB \rightarrow X + (AB^-)^{\#} \rightarrow X + AB^{\#} + e^- \quad (CTSR)$$

$(AB^-)^{\#}$ represents the TNI resulting from the electron transfer, which can be electronically and/or rovibrationally excited, while $AB^{\#}$ represents the neutral (excited) molecular target. Whereas the equation does not show X in an excited state, we do not disregard that possibility.

Previous studies of these collision systems [5–10] mostly focus on discrimination between DD and CTSR. Hence it has been shown that DD results in very low energy loss by the projectile (≤1 eV) while CTSR is characterized by higher energy losses (around 3–4 eV). Furthermore, these studies show that, while at lower projectile collision energies (up to ~100 eV, i.e., $v/v_{Bohr} \approx 0.063$) direct detachment dominates [7], CTSR becomes increasingly significant at gradually higher energies [7] (i.e., $v/v_{Bohr} > 0.2$). Conversely, fragmentation processes have received little attention. The lifetime of the TNI has to be sufficiently long for fragmentation channels to be able to compete with electron detachment through CTSR. The role of collisional excitation in TNI formation in anion–molecule collisions has not been investigated in the literature.

In the present work, the anion mass spectra will be largely based on comparisons with free electron attachment studies. Similarities with free electron attachment results are expected in the case of electron transfer from H^- since its *extra* electron is relatively loosely bound (0.75 eV [11]) and hence may be considered to approximate a free electron [7,8]. For this model to be valid, the collision velocity has to be much higher than the electron velocity in the projectile frame. In the case of H^-, this is achieved for collision energies much higher than 1.5 keV [8]. In the present study, the highest collision was 4 keV and therefore the application of this model has to be made carefully. However, a classical picture can be used for collision energies in this energy range [8]. As is explained in the studies of Refs. [5,7,8], the electron can be considered to have a broad energy distribution between $\upsilon_e - \upsilon_i$ and $\upsilon_e + \upsilon_i$, where υ_e is the velocity of the H^- system and υ_i is the velocity of the bound electron in the ion frame. As such, for a 1 keV H^- collision energy, an analogy can be made with free electrons with an impact energy distribution between 0.02 and 2.56 eV. Due to higher ion mass and also higher binding energies of the extra electron, the model is not useful to analyse the present O^- and OH^- impact results.

In Table 1 the ion velocities for the several projectiles used in this study are presented. The velocity values are presented in Bohr velocity units and are obtained through:

$$\frac{v}{v_0} \approx 6.325\sqrt{E}$$

where v/v_0 is the velocity of the ion relative to the Bohr velocity and E is the energy per mass unit in MeV/a.m.u. As is the case for anionic products, the literature surrounding cation production in collisions with anion projectiles is quite scarce. For velocities significantly higher than the Bohr velocity of the electron ($v \gg v_{Bohr}$), cross section measurements for single and double ionization of He and Ar by 0.5–2 MeV H^- impact (4.5–8.9 v_{Bohr}) have been performed [12]. Further experiments have probed target ionization, projectile scattering, and projectile electron loss in 1 MeV H^- collisions with He atoms [13]. At intermediate velocities ($v \approx v_{Bohr}$), single and double ionization of He, Ar, N_2, and H_2 targets has been analysed following collisions with anion projectiles (B^- F^-, C^-, and O^-) [14–16]. These studies indicate the dissociative ionization is dominant for low impact parameters (more *direct* collisions generally with higher momentum transfer), whereas non-dissociative ionization (i.e., formation of the parent cation) dominates at higher impact parameters. At lower impact velocities ($v \ll v_{Bohr}$), electron loss from H^- projectiles with electronic excitation of the resultant H^0 has been studied in 1–5 keV (0.20–0.45 v_{Bohr}) collisions with rare gas atoms and N_2 molecules [17]. Minimal H^- impact energy dependence was observed in the cross sections for excitation to H (3*d*), H (3*s*), H (4*s*), and H (5*s*) states. Furthermore, Geddes et al. [18] measured cross sections for the formation of excited ($n = 2$ or 3) hydrogen atoms in 3–25 keV (0.35–1.00 v_{Bohr}) H^- ions with H, H_2, He, Ne, Ar and N_2. Stone and Morgan [19] recorded cross sections for hydrogen excitation to highly excited states ($12 \leq n \leq 28$) in 2.8–60 keV (0.33–1.55 v_{Bohr}) H^- collisions with H, H_2, and Ar. Significantly, the cross sections for electron loss by H^- show contrasting trends in 0.1–10 keV (0.06–0.63 v_{Bohr}) [20] collisions with H and H_2. With increasing H^- impact velocity, the electron loss cross sections decrease for collisions with H whereas they increase to an apparent maximum at ~0.6 v_{Bohr} for H_2.

2. Experimental set-up

The experimental set-up used in this study consisted of a cross beam technique, where gas phase molecules interact with anion projectiles. The anion beam was produced in a PS-120 Negative Ion Caesium Sputter Source from Peabody Scientific™, operating between 1 and 4 keV. The beam emerging from the source was focused by an electrostatic lens system and momentum analysed by a 90° double focusing magnet. After further focusing and collimation the beam was directed into the interaction chamber where it crossed an effusive beam of gas phase molecules derived from liquid samples. A cycle of freeze-thawing steps was carried out on the

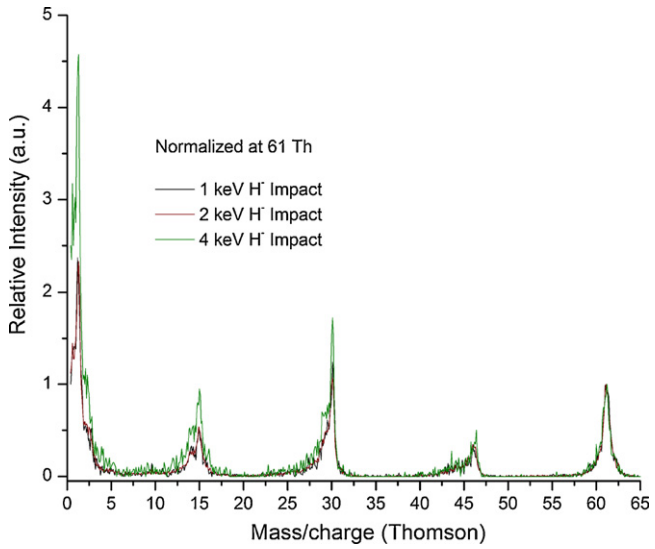

Fig. 1. Mass spectra of cations produced in 1–4 keV H^- collisions with gas-phase nitromethane. The data has normalized such that the intensities of the $CH_3NO_2^+$ (parent cation) peaks are equal.

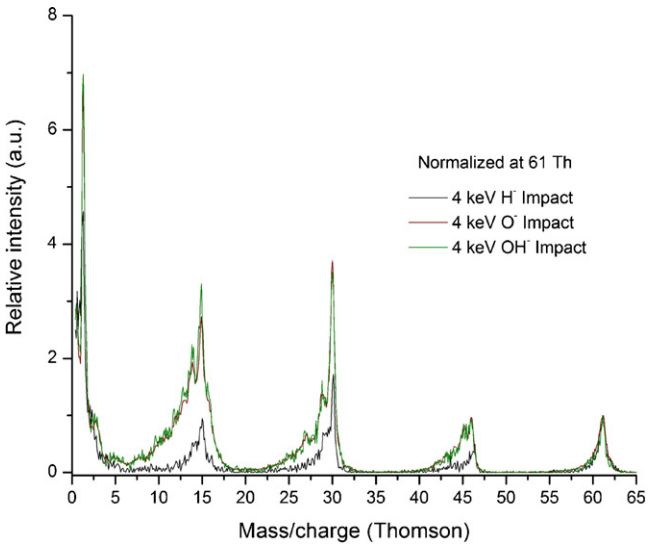

Fig. 2. Mass spectra of cations produced in 4 keV H^-, O^-, and OH^- collisions with gas-phase nitromethane. The data has been normalized such that the intensities of the $CH_3NO_2^+$ (parent cation) peaks are equal.

liquid samples to remove any dissolved gases and ensure a pure gas target. Cationic or anionic fragments were extracted from the interaction region into an orthogonal quadrupole mass spectrometer. Notwithstanding the relatively low m/q resolution, clear distinctions can be made throughout the presented spectra and specific issues regarding this matter are discussed more thoroughly in the corresponding section. Anion currents were measured in a Faraday cup after the collision region. The low background pressure of 10^{-7} mbar in the interaction chamber resulted in a negligible background contribution to the mass spectra. The target pressures used ensured single collision conditions in the interaction region and negligible secondary collisions of the fragment ions. Ion extraction voltages of approximately 25 V cm^{-1} were applied in order to prevent any deflection of the anionic beam into the differentially pumped quadrupole mass spectrometer. The mass spectra were normalized to both total extraction times and beam currents.

3. Results and discussion

3.1. Cation formation

3.1.1. Nitromethane (CH_3NO_2)

Generally speaking, the same main *groups* of cations were observed for the various ionization methods (anion impact, fast electron impact, and photoionization). In particular, the local maxima for each group in the present data agree with those in the previous work. The absence of some weak features in the present data can be explained by relatively low signal-to-noise ratios. Additionally, a general overview of the spectra shows that for all impact energies and projectiles, the major peaks are always the same for the corresponding target molecule.

Fig. 1 shows mass spectra at different H^- projectile energies (1, 2 and 4 keV), while Fig. 2 compares spectra for different projectiles. The yields in both figures are normalized to the parent cation, therefore creating a clearer picture of the relative amount of dissociative ionization versus the parent cation production. Indeed, it is clear from Fig. 1 that for higher projectile energies, the relative amount of fragmentation is higher. This indicates increased statistical fragmentation associated with greater energy deposition. Indeed, the relative production of fragment cations is markedly greater for 4 keV H^- impact, with new resolved peaks visible at 45 and 29 Thomson. This suggests energy transfer distributions that are similar at 1 and 2 keV but distinctly higher at 4 keV.

Fig. 2 shows that the ratio of fragment cation production/$CH_3NO_2^+$ production is much greater for 4 keV O^- and OH^- impact than for H^- impact. However at impact kinetic energies (KE) that are significantly greater than the thresholds for the various ionization pathways, collision velocity is generally recognized as a more significant parameter than projectile KE for the interpretation of ionization results (notably in relation to energy deposition and branching ratios for dissociative ionization/total ionization). Hence the reason for the observed differences in the present nitromethane mass spectra produced by H^- impact (1–4 keV, 0.20–0.40 v_{Bohr}) and by O^- and OH^- impact (4 keV, 0.010 v_{Bohr}) is not totally clear; the velocities are different as well as the projectiles. As H^- has the weakest outermost electron binding energy (0.75 eV), reduced fragmentation by H^- impact appears to be broadly consistent with the generalized association of smaller impact parameters (more *direct* collisions, smaller cross sections) with greater energy deposition and hence increased fragmentation [14,15,21,22]. Similarly, Fig. 2 shows a subtle increase in fragmentation for OH^- impact compared with O^- (binding energies of the outermost electrons in the respective anions: 1.92 and 1.46 eV). More generally, however, both Figs. 1 and 2 are consistent with a possible relation between increased projectile momentum and increased relative production of fragment ions.

3.1.2. Methanol (CH_3OH), ethanol (C_2H_5OH) and water (H_2O)

Fig. 3 shows mass spectra of methanol (CH_3OH) as a function of incident O^- and OH^-, while the observed cationic fragments are listed in Table 2

. Apart from H^+ formation, the dominant fragments are the dehydrogenated parent cation and its parent precursor. It is interesting to note that a comparison with electron ionization spectra [23] provides a very similar picture. As is the case of nitromethane, collisions of heavier projectiles at the same KE (hence higher momentum) favour dissociative ionization in detriment of non-dissociative ionization, consistent with the interpretation mentioned above.

Mass spectra for 4 keV H^-, O^- and OH^- impact on ethanol (C_2H_5OH) are presented in Fig. 4 and the identified cationic fragments are summarized in Table 2. As observed for methanol, the fragmentation pattern closely resembles the electron impact

Table 2
Cations produced in the present collisions (1–4 keV H^- impact, 4 keV O^- impact, and 4 keV OH^- impact) compared with examples of previous electron impact and photoionization data. It is noteworthy that for all impact energies and projectiles the same major peaks were observed.

	Resolved cation masses (m/q)			Proposed assignments and appearance energies (eV)
	Present work	Electron impact [11] [a]	375 nm (3.31 eV) multi-photon ionization [44]	
Nitro-methane CH_3NO_2	61[b]	61[b]	61[b]	$CH_3NO_2^+$ (11.08 [11,23])
		60	60	$CH_2NO_2^+$ (11.8 [45])
	46[b]	46[b]	46[b]	NO_2^+ (12.1 [45])
	45[c]	45	45	CH_3NO^+
		44	44	CH_2NO^+ (11.75 [45])
		43	43	$CHNO^+$
		42	42	CNO^+
		31	31	NOH^+
	30[b]	30[b]	30[b]	NO^+ (11.75 [45])
	29[c]	29	29	CHO^+/CH_3N^+
		28	28	CO^+/CH_2N^+
		27	27	CHN^+
		26		CN^+
		16	16	O^+ (14.50 [46])
	15[b]	15[b]	15[b]	CH_3^+ (12.6 [47])
	14	14	14	N^+/CH_2^+
		13	13	CH^+
		12	12	C^+ (22.83[46])
			2	H_2^+
	1		1	H^+
	Present work	Electron impact [11] [a]	288.3 eV photoionization [40]	Proposed assignments and appearance energies (eV)
Methanol CH_3OH	32	32	32	CH_3OH^+ (10.84 [11])
	31[b]	31[b]	31[b]	CH_3O^+ (11.649 [41])
	30	30	30	CH_2O^+ (12.05 [42])
	29	29	29	CHO^+ (13.06 [42])
		28	28	CO^+ (13.7 [43])
			18	H_2O^+
	17		17	OH^+ or CH_4^+
			16	O^+
	15[b]	15[b]	15[b]	CH_3^+ (13.82 [42])
	14[d]	14	14	CH_2^+ (14.05 [42])
			13	CH^+
			12	C^+
			3	H_3^+
			2	H_2^+
	[b]		[b]	H^+
	Present work	Electron impact [11] [a]	292 eV photoionization[40]	Proposed assignments and appearance energies (eV)
Ethanol C_2H_5OH	46	46	4[b]	$C_2H_5OH^+$ (10.48 [11])
	4[b]	45[b]	45	$C_2H_5O^+$ (10.801 [48])
	44[d]		44	$C_2H_4O^+$ (10.45 [49])
	43[d]	43	43	$C_2H_3O^+$ (14.5 [43])
	42	42	42	$C_2H_2O^+$
			41	C_2HO^+
			40	C_2O^+
			32	CH_4O^+
	31[b]	31[b]	31[b]	CH_3O^+ (11.25 [50])
	30[d]	30	30	CH_2O^+ (11.70 [51])
	29[d]	29	29	CHO^+ or $C_2H_5^+$
	28[d]	28	28	$C_2H_4^+$ (12.0 [50])
	27[d]		27	$C_2H_3^+$ (14.7 [43])
	26[d]	26	26	$C_2H_2^+$
		25	25	C_2H^+
	19[d]	19	19	H_3O^+ (13.8 [52])
			18	H_2O^+
			17	OH^+
			16	O^+
	15[b,e]	15[b]	15[b]	CH_3^+ (14.70 [53])
	14[b,e]	14	14	CH_2^+
		13	13	CH^+
			12	C^+
			2	H_2^+
	[b]		1	H^+ (21.0 [54])

Table 2 (*Continued*)

	Present work	Electron impact [37] [a]	21.23 eV photoionization [55]	Proposed assignments and appearance energies (eV)
Water H_2O	18	1[b]	1[b]	H_2O^+ (13.5)
	17	17	17	OH^+ (17.5)
	16	16	16	O^+ (25)
		16		O^{++} (90)
		2		H_2^+ (30)
	1	1		H^+ (20)

[a] Impact energy unspecified (typically ~70 eV).
[b] Local maximum.
[c] Only resolved for 4 keV anion impact.
[d] Only resolved for O^- and OH^- impact.
[e] Similar intensities.

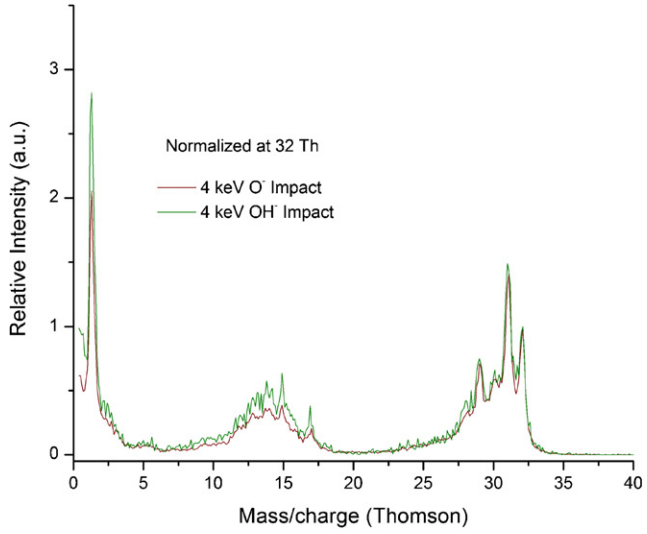

Fig. 3. Mass spectra of cations produced in 4 keV H^-, O^-, and OH^- collisions with gas-phase methanol. The data has been normalized such that the intensities of the CH_3OH^+ (parent cation) peaks are equal.

ionization data [23]. Moreover, the ratio of fragment cation production/$C_2H_5OH^+$ production increases gradually with projectile mass (i.e., H^- to OH^-). Once more it would appear that the key parameter to consider is the momentum of the projectile rather than its energy [14,15,21,22].

Finally, Fig. 5 presents mass spectra of cations produced in 4 keV H^-, O^- and OH^- collisions with water. As observed in the equivalent data for nitromethane, ethanol, and methanol, no significant difference exists between O^- and OH^- collisions, whereas for H^- collisions it is clear that the relative H^+ yield is significantly lower (Table 3).

3.2. Anion formation

3.2.1. Nitromethane (CH_3NO_2)

Nitromethane anion formation has been studied in the gas-phase by free electron attachment [24,25], in alkali atom collisions [2] and in Rydberg electron transfer studies [26]. Of the molecules studied, nitromethane is the only one with a sufficiently large dipole moment (above the critical value of ~2.5*D* [27]) to bound an extra electron in a stable dipole-bound state, potentially playing a significant role in the collisions dynamics. In free electron attachment studies, the dominant fragment was NO_2^- and no parent anion ($CH_3NO_2^-$) was observed. This is reasonable due to the small positive electron affinity of CH_3NO_2. In the present study, we observed the parent anion $CH_3NO_2^-$ as the dominant fragmentation pathway for all collision energies (Fig. 6) and for all the different electron donors (H^-, O^- and OH^-, Fig. 7). The other, less intense, detected fragments were NO_2^- and H^-. As a comparison, results obtained in alkali atom collision experiments have shown that the main fragment was reported to be NO_2^- but, in contrast to free electron attachment studies, the creation of the parent anion

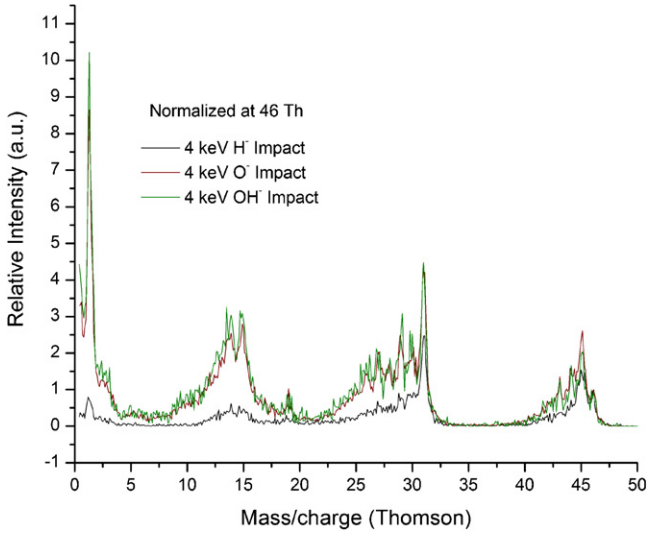

Fig. 4. Mass spectra of cations produced in 4 keV H^-, O^-, and OH^- collisions with gas-phase ethanol. The data has been normalized such that the intensities of the $C_2H_5OH^+$ (parent cation) peaks are equal.

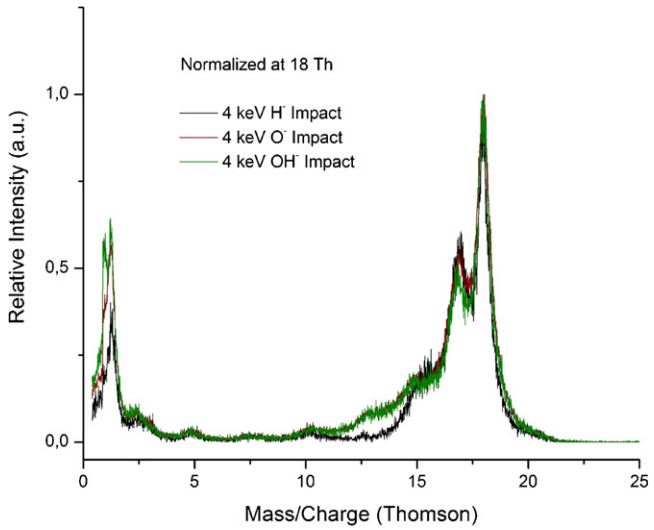

Fig. 5. Mass spectra of cations produced in 4 keV H^-, O^- and OH^- collisions with gas-phase water. The data has been normalized to the parent cation.

Table 3
Anionic fragmentation products for the several target molecules. The different projectiles do not yield different products.

	Present work	Free electron attachment [38]	Proposed assignments
Water H_2O	17	17	OH^-
	16	16	O^-
	1	1	H^-

	Present work	Free electron attachment [33,36]	Proposed assignments
Methanol CH_3OH[b,c]	32[a]		CH_3O^-
	31	31	OH^-
	17[d]	17	OH^-
	16	16	O^-
	14		CH_2^-
	1	1	H^-

	Present work	Free electron attachment [34]	Proposed assignments
Ethanol C_2H_5OH[b]	45	45	$CH_3CH_2O^-$
	44		$C_2H_4O^-$
	43		$C_2H_3O^-$
	32		CH_3OH^-
	17	17	OH^-
	16	16	O^-
	15		CH_3^-
	14		CH_2^-
	1	1	H^-

	Resolved anion masses (m/q)			Proposed assignments
	Present work	Free electron attachment [24,25]	Alkali atom collisions [2]	
Nitromethane CH_3NO_2	61[a]		61	$CH_3NO_2^-$
	60	60	60	$CH_2NO_2^-$
		59		$CHNO_2^-$
		47		$^{15}NO_2^-$
	46	46[a]	46[a]	NO_2^-
	45[d]			CH_3NO^-
		44		CH_2NO^-
		42	42	CNO^-
		32		H2NO$^-$
		30	30	NO^-
		26	26	CN^-
		18		$^{18}O^-$
		17	17	OH^-
	16	16	16	O^-
		15		CH_3^-
		14		CH_2^-
		13		CH^-
	1	1	1	H^-

[a] Local maximum.
[b] Only resolved for 4 keV anion impact.
[c] Only resolved for O^- and OH^- impact.
[d] Extrapolated.

$CH_3NO_2^-$ was observed. As stated before, within the set of molecules investigated in this work, nitromethane stands out due to the presence of a stable dipole-bound anionic state [28], which has been shown both experimentally and theoretically to provide a doorway into valence states of the molecular parent anion [26,29]. This initial dipole-bound molecular anion possesses a significantly different geometry than its neutral counterpart (a symmetric bend of the oxygen atoms in the $-NO_2$ group resulting in a tetrahedral shape [30]).

Similarly to both alkali atom collisions and Rydberg electron transfer, nitromethane parent anion formation by negative ion impact is expected to proceed through a transition to a low vibrational state of a $^2B_1$ anionic state, whereas this does not occur in free electron attachment interactions [31,32]. From a different point of view, this mechanism may rely on an interaction of the projectile donor and the molecule, modifying the relative position or shape of the potential surfaces and thereby changing the dissociation pathway. Owing to the high dipole moment of nitromethane, the presence of H, O or OH in the collision complex may be rationalised as a third body "forcing" the electron to remain in the dipole-bound state long enough for the molecule to adiabatically proceed into its anionic geometry, thereby transferring by intramolecular relaxation the electron into one of its valence orbitals (in the anionic geometry). This is in contrast with free electrons where, even if the electron is initially captured into the dipole-bound state, its lifetime is not long enough to compete with necessary molecular deformation from the neutral to the anionic geometry, yielding considerable auto-detachment.

In free electron attachment studies, the creation of NO_2^- arises from a vertical transition of 0.6 eV from the neutral ground state of the molecule to a $^2B_1$ (π^*) symmetry state of the anionic molecule [2]. At this stage, due to an avoided crossing between this state and a dissociative $^2A_1$ (σ^*) anionic state, tunnelling can occur through the formed barrier, thereby yielding NO_2^-. Another possibility for the formation of NO_2^- would be a direct transition to this $^2A_1$ (σ^*) anionic state. However, a vertical transition to this orbital would lie inside the curve of the neutral state, thereby most likely resulting in auto-detachment. By contrast, in alkali atom collision studies, NO_2^- is attributed to an initial transition to the aforementioned $^2A_1$ (σ^*) dissociative state, mainly through an ionic scattering. The presence

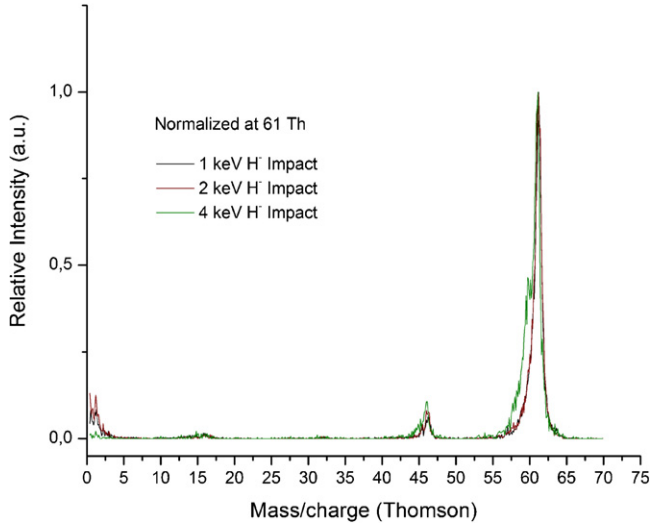

Fig. 6. Mass spectra of anions produced in 1, 2 and 4 keV H^- collisions with gas-phase nitromethane. The data has been normalized to the parent anion (61 Th).

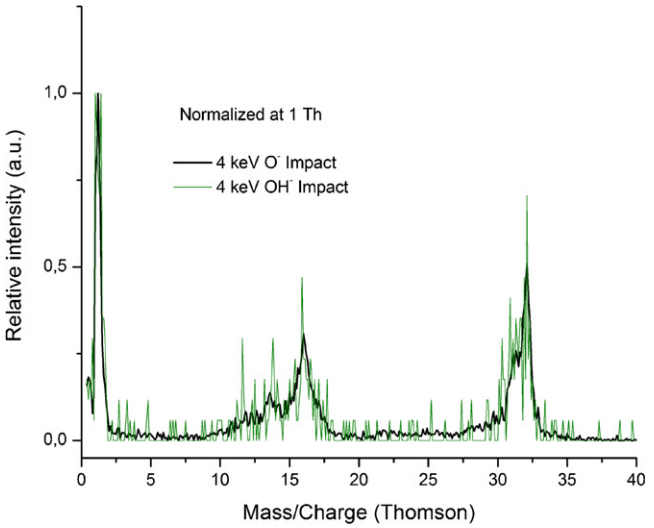

Fig. 8. Mass spectra of anions produced in 4 keV O^- and OH^- collisions with gas-phase methanol. The data has been normalized to 1 Th.

of the alkali cation allows the temporary negative anion (TNI) to relax into a geometry below the neutral state, thereby precluding auto-detachment and allowing for the dissociation of the TNI into NO_2^- [31,32].

When compared with free electron attachment and K impact, the present data show very low yields of NO_2^- relative to the parent anion and its dehydrogenated anion. This indicates that a direct and unilateral comparison with either free electron attachment or alkali atom collisions is not sufficient to explain the results. Indeed, the fact that the NO_2^- yield is very low appears to indicate that NO_2^- formation both through initial capture into $^2B_1$ (free electron attachment pathway) or into $^2A_1$ (electron transfer pathway) states are either suppressed or results mostly in auto-detachment.

As mentioned above, the formation of NO_2^- from a vertical transition to the $^2A_1$ dissociative curve can only occur if dissociation successfully competes with auto-detachment. The presence of the potassium cation in alkali atom collisions accomplishes this suppression [2]. However, since we do not obtain a significant yield of NO_2^- in the present measurements, the presence of the hydrogen radical does not appear to provide stabilization with respect to a vertical transition to the $^2A_1$ curve. Hence this suggests that auto-detachment suppression in alkali atom–molecule collisions is indeed due to a coulombic interaction between the electron donor and the target molecule. This lends support to the rationale of considering an ionic ($K^+ + CH_3NO_2^-$) transient complex during the collision time for potassium–nitromethane collisions.

On the other hand, the inability to produce NO_2^- from an initial capture to the $^2B_1$ state can imply that the tunnelling mechanism shown to explain the NO_2^- formation with free electrons is somehow suppressed [2,31,32]. Indeed, if the asymptotic value of the $^2A_1$ curve is higher than the final vibrational state of the $(CH_3NO_2^-)^\#$ transient anion, no such tunnelling effect is possible. This interpretation suggests that, whereas with free electrons the transition to the anionic state can be considered vertical (Franck-Condon), this is not necessarily the case for electron transfer mechanisms, neither for ion-pair formation nor in the present experiments.

As can be seen in Fig. 6, higher projectile energies seem to favour formation of higher mass fragments, namely NO_2^-. Fig. 7 presents spectra with the same collision energies but different projectiles. A direct comparison shows that higher mass projectiles favour dissociation.

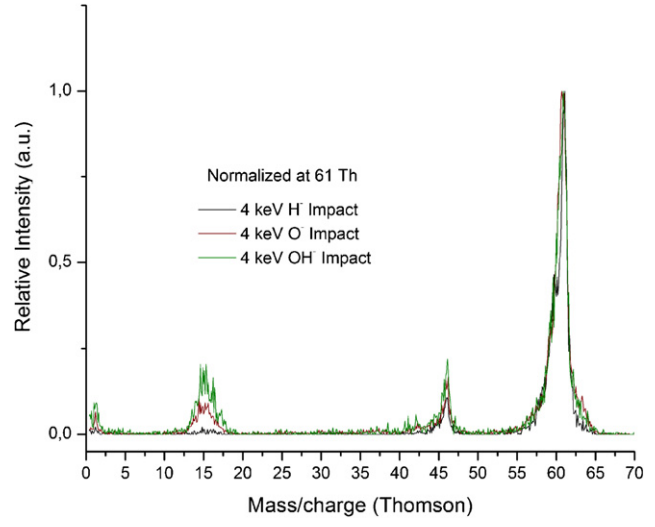

Fig. 7. Mass spectra of anions produced in 4 keV H^-, O^- and OH^- collisions with gas-phase nitromethane. The data has been normalized to the parent anion (61 Th).

3.2.2. Methanol (CH_3OH)

As the simplest methyl alcohol, free electron attachment studies of methanol have been extensively performed [33,35,36]. In these studies, O^-, OH^- and the dehydrogenated parent anion (CH_3O^-) are the main fragments [33] and the hydride anion was also found to be a major fragmentation product [35,36], sharing the same resonances as CH_3O^-. All of the fragments have been attributed to core-excited resonances since their energetic thresholds (2.1, 2.4 and 2.9 eV for O^-, OH^- and CH_3O^-, respectively) [33] are much lower than the obtained resonance profiles.

As in the free electron attachment studies, the main fragments in the present O^- and OH^- impact experiments on methanol are H^-, O^-, OH^- and CH_3O^- (Fig. 8). As for the 32 Th signal that may correspond to the parent anion (CH_3OH^-), this has neither been detected in free electron attachment studies nor in any other previous negative ion studies [33,35]. This is reminiscent of the rather small vertical electron affinity (~0 eV) of methanol.[1] Though, we do not discard the possibility of an O_2^- contribution. In any case electron

[1] M. Probst, *private communication* where the DFT calculated vertical electron affinities for the trans and cis geometry of ethanol are 0.02 and 0.63 eV, respectively.

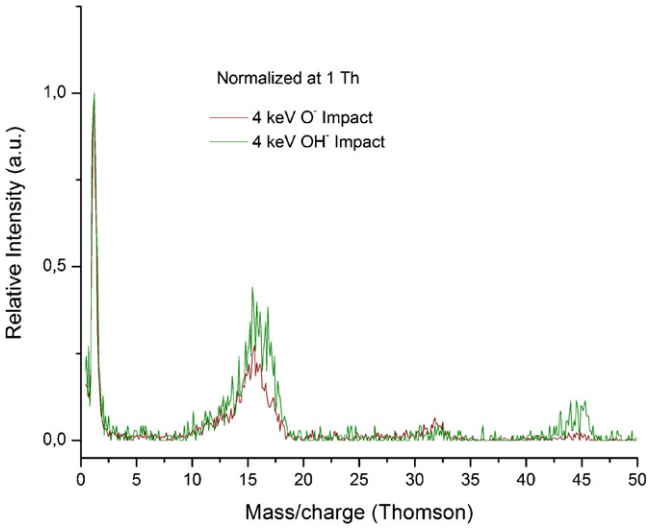

Fig. 9. Mass spectra of anions produced in 4 keV O^- and OH^- collisions with gas-phase ethanol. The data has been normalized to 1 Th.

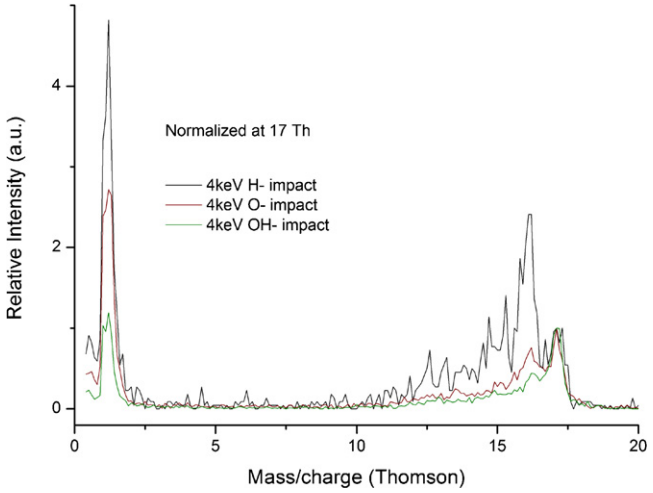

Fig. 10. Mass spectra of anions produced in 4 keV H^-, O^- and OH^- collisions with gas-phase water. The data has been normalized to 17 Th.

transfer experiments (e.g., with alkalis) will be shortly performed in our laboratory in order to further investigate the presence of this anion in the context of atom–molecule collisions.

3.2.3. Ethanol (C_2H_5OH)

The main fragments produced in recent free electron attachment experiments are O^-, OH^- and the dehydrogenated parent anion $CH_3CH_2O^-$, with no detection of the parent anion $CH_3CH_2OH^-$ [34]. These studies report that the resonances for those fragments are lower in energy but still well above the energy thresholds, similar to the methanol results [33,34].

The present OH^- and O^- impact experiments on ethanol produced H^-, O^-, OH^- and $CH_3CH_2O^-$ fragments (Fig. 9). Comparing the relative anion yields of O^-, OH^- and $CH_3CH_2O^-$ in free electron attachment studies with the relative intensities in this work reveals that they have approximately similar values. Furthermore, as in the case of methanol, H^- formation is obtained in the present studies but no information regarding the accessible resonant states through free electron attachment is available. Finally, a small but rather clear structure appears at 32 Th, which can be attributed to methanol (CH_3OH^-). The exact origin of this anion cannot be unambiguously determined. One possibility is the formation of this anion by abstraction of the methyl together with a hydrogen transfer. However, another more straightforward explanation is the presence of methanol as an impurity in the sample or in the sample admission system. As in methanol, the possibility of O_2^- contribution should also be considered. Further studies in the future will help clarifying this issue.

3.2.4. Water (H_2O)

Studies of electron attachment in water have been quite extensively performed. An extensive review on this ubiquitous molecule has been published recently [37]. The reported fragmentation consists of H^-, O^- and OH^- [37,38]. H^- formation is predominantly from a rather broad resonance at 6.4 eV and another less broad resonance at 8.24 eV, which is shared with formation of O^- and OH^-. The formations of these two anions share the same resonances (at 6.4, 8.24 and ~11.5 eV), though with different cross sections [37,38].

Compared with the pseudo-free electron energy (2.2 eV) for a 4 keV H^- projectile, the free electron attachment resonance energies are all high even when the velocity of the bound electron in the ion frame is taken into account, giving the range 0.38–5.58 eV (see Section 1). Therefore, the pseudo free electron analogy would lead us to expect negligible formation of any of these product anions. However these free electron attachment profiles are reminiscent to core-excited resonances and so their contributions may deviate from the assumptions drawn for low energy resonances (typically below 3–4 eV) in the model. At this point, it is quite interesting to note that, in H^- collision studies with N_2, a higher energy structure in the H energy loss spectra appears around the 10 eV region, which the authors attribute to "collisional excitation" [7]. Water, methanol and ethanol share the fact that their fragmentation stems from core-excited resonances. Furthermore, electron transmission spectroscopy studies performed on N_2 show the presence of core-excited resonances within the 8–11 eV energy range [39] thereby indicating that the "collisional excitation" brought forward in the anion collision studies may indeed be due to core-excited resonances. The quasi-free electron attachment model developed in the aforementioned studies [8–10] most likely does not encompass these core-excited resonances.

We report the formation of 1, 16 and 17 Th fragments, as shown in Fig. 10, assigning them to H^-, O^- and OH^-, respectively. Similarly to free electron attachment, H^- formation is the dominant fragment for all projectiles, although its yield is comparable to the other fragments, which is not in agreement with the ionic yields in free electron attachment, where H^- is one order of magnitude higher than O^- and two orders of magnitude higher than OH^- [37,38].

The most interesting fragment however is OH^-. As can be seen in Fig. 10, OH^- yield increases significantly for increasing mass of the projectile. For H^- collisions, the OH^- yield is distinctly lower than the yield for O^- formation. In O^- collisions, the O^- and OH^- yields are approximately the same and finally, for OH^- collisions, OH^- yield is significantly higher than the O^- yield.

For H^- collisions, the OH^- yield is low compared with its yield for O^- and H^- formation with this projectile. Hence the present H^- impact data is more similar to the free electron attachment data[38] than the OH^- and the O^- impact data, as generally expected on the basis of the pseudo free electron rationale. Further investigations are necessary to identify the mechanisms leading to the strong OH^- and O^- product ion channels in the present heavier anion projectile data. It is worth noting that the timescale of the present collisions (tens of femtoseconds) is too short for proton transfer processes to take place.

4. Conclusions

In this work we have measured mass spectra for both anion and cation production for anion collisions (H^-, O^- and OH^-) with several organic compounds. For all the molecules studied (nitromethane, methanol, and ethanol) the product cations were consistent with mass spectra observed using alternative energy deposition mechanisms (notably electron impact ionization), however differences were observed in terms of the relative intensities. The relative production of fragment cations/parent cations from nitromethane in collisions with H^- increased as a function of impact velocity in the range 0.01–0.40 v_{Bohr}. At constant anion impact energy (4 keV), fragmentation increased with the mass of the projectile anion in the sequence ($OH^- > O^- > H^-$). A possible common interpretation for both these results is to associate higher projectile momentum with increased energy deposition in the collisions. No clear evidence was observed for effects on the mass spectra due to the binding energy of the projectile anion's outermost electron. However, it has to be noted that some of the fragments not observed in this study may simply be due to the poor statistics and resolution of the quadrupole system, rather than to suppression of the fragmentation pathway.

In the case of negative ion formation, both methanol and ethanol show fragmentation patterns that closely resemble free electron attachment, although a significant signal of the parent anion in methanol is also observed. In the case of nitromethane, the fragmentation is significantly different from that obtained both in free electron attachment and in alkali atom–molecule collisions. It is quite interesting to note that the low yield of NO_2^- lends credibility to the assumption that the stabilizing effect produced by the potassium cation in alkali atom collisions [2,32] stems from the electrostatic interaction between the potassium cation and the molecular TNI [2]. This mechanism has also been reported with biological molecules elsewhere [3,4]. As far as water is concerned, the reason for the increased yield of OH^- for higher mass projectiles is still not clear.

Finally, one of the main issues surrounding the analysis of the presented spectra pertained to inability of the quasi-free electron model to explain the appearance of fragments that require energies significantly above the ones obtained through it. By analysing data regarding N_2 [7,39], it was proposed in this study that the processes of collisional excitation described in Ref. [7] can actually correspond to core-excited resonances. By extending this rationale to the molecules studied herein, the formation of the fragments that show thresholds higher than the energy range allowed by the classical quasi-free electron model can also be explained through the access to core-excited resonances.

In summary, the present spectra show that the fragmentation channels of these anion–molecule collisions can be very different from those obtained both in free electron attachment and in electron transfer. However, as expected from the pseudo-free electron approximation, the H^- projectile anion mass spectra from nitromethane and water better resemble the previous free electron attachment data than the mass spectra for OH^- and O^- projectiles. It is worth noting that the fragmentation of water, ethanol and methanol has previously been shown to stem from core-excited resonances [33,34,36,38]. Future work exploring these mechanisms in anion–molecule collisions may provide some answers regarding the limitations of the quasi-free electron model.

Acknowledgements

The authors wish to acknowledge the ITS-LEIF network, Ion Technology and Spectroscopy with Low Energy Ion beam Facilities, Transnational Access, Integrating Activities and Accompanying Measures, Integrated Infrastructure Initiative-I3, 6th FP, ITS LEIF-BH-2005-003, 2006–2009. D.A. and R.A. wish to acknowledge the Portuguese Foundation for Science and Technology (FCT-MCTES) for post-graduate scholarships SFRH/BD/61645/2009 and SFRH/BD/32271/2006, respectively. S.E. acknowledges the exchange visit to the Universidade Nova de Lisboa during the analytical stage of this research. S.E. and P.L.V. acknowledge the support from the British Council for the Portuguese-English joint collaboration. S.E. acknowledges the support of the British EPSRC through the Life Sciences Interface Fellowship program and of the European Commission through a Marie Curie Intra-European Reintegration Grant. We also acknowledge Professor Michael Probst from the University of Innsbruck for providing his DFT calculations on the vertical electron affinities. PLV acknowledges the visiting fellow position at the Department of Physics and Astronomy, The Open University, UK. This work forms part of EU COST Action CM0601 and CM0805 programmes "ECCL" and "The Chemical Cosmos", respectively.

References

[1] V. Vuitton, P. Lavvas, R.V. Yelle, M. Galand, A. Wellbrock, G.R. Lewis, A.J. Coates, J.E. Wahlund, Planet. Space Sci. 57 (2009) 1558–1572.
[2] R. Antunes, D. Almeida, G. Martins, N.J. Mason, G. Garcia, M.J.P. Maneira, Y. Nunes, P. Limao-Vieira, Phys. Chem. Chem. Phys. 12 (2010) 12513–12519.
[3] F. Ferreira da Silva, D. Almeida, R. Antunes, G. Martins, Y. Nunes, S. Eden, G. Garcia, P. Limão-Vieira, Phys. Chem. Chem. Phys 13 (2011) 21621–21629.
[4] D. Almeida, R. Antunes, G. Martins, S. Eden, G. Garcia, F. Ferreira da Silva, Y. Nunes, P. Limao-Vieira, Phys. Chem. Chem. Phys. 13 (2011) 15657–15665.
[5] T. Okamoto, Y. Sato, H. Inouye, Phys. Rev. Lett. 52 (1984) 184–187.
[6] V.N. Tuan, J.P. Gauyacq, V.A. Esaulov, J. Phys. B-At. Mol. Opt. 16 (1983) L95–L98.
[7] V.N. Tuan, V.A. Esaulov, J. Phys. B-At. Mol. Opt. 15 (1982) L95–L100.
[8] V.N. Tuan, V. Esaulov, J.P. Gauyacq, A. Herzenberg, J. Phys. B-At. Mol. Opt. 18 (1985) 721–735.
[9] V.N. Tuan, V. Esaulov, J.P. Guayacq, J. Phys. B-At. Mol. Opt. 17 (1984) L133–L137.
[10] V.N. Tuan, V.A. Esaulov, J.P. Grouard, R.I. Hall, J.L. Montmagnon, J. Phys. B-At. Mol. Opt. 17 (1984) 2897–2912.
[11] NIST, NIST Chemistry WebBook, http://webbook.nist.gov.
[12] J. Sorensen, L.H. Andersen, L.B. Nielsen, J. Phys. B-At. Mol. Opt. 21 (1988) 847–858.
[13] J.P. Giese, E. Horsdal, Nucl. Instrum. Meth. B 40-1 (1989) 201–204.
[14] F. Zappa, A.L.F. de Barros, L.F.S. Coelho, G. Jalbert, S.D. Magalhaes, N.V.D. Faria, Phys. Rev. A (2004) 70.
[15] A.L.F. de Barros, S. Martinez, F. Zappa, S. Suarez, G. Bernardi, G. Jalbert, L.F.S. Coelho, N.V.D. Faria, Phys. Rev. A (2005) 72.
[16] M.M. Sant'Anna, Braz. J. Phys. 36 (2006) 518–521.
[17] M. Harnois, R.A. Falk, R. Geballe, J. Risley, Phys. Rev. A 16 (1977) 2256–2263.
[18] J. Geddes, J. Hill, H.B. Gilbody, J. Phys. B-At. Mol. Opt. 14 (1981) 4837–4846.
[19] J.A. Stone, T.J. Morgan, Phys. Rev. A 31 (1985) 3612–3619.
[20] M.W. Gealy, B. Vanzyl, Phys. Rev. A 36 (1987) 3091–3099.
[21] R. Cabrera-Trujillo, J.R. Sabin, Y. Ohrn, E. Deumens, Phys. Rev. Lett. 84 (2000) 5300–5303.
[22] R. Cabrera-Trujillo, Y. Ohrn, E.S. Deumens Jr., Phys Rev A (2000) 62.
[23] S.G. Lias, NIST Chemistry WebBook, NIST, 2009.
[24] W. Sailer, A. Pelc, S. Matejcik, E. Illenberger, P. Scheier, T.D. Mark, J. Chem. Phys. 117 (2002) 7989–7994.
[25] E. Alizadeh, F.F. da Silva, F. Zappa, A. Mauracher, M. Probst, S. Denifl, A. Bacher, T.D. Mark, P. Limao-Vieira, P. Scheier, Int. J. Mass Spectrom. 271 (2008) 15–21.
[26] R.N. Compton, H.S. Carman, C. Desfrancois, H. AbdoulCarmine, J.P. Schermann, J.H. Hendricks, S.A. Lyapustina, K.H. Bowen, J. Chem. Phys. 105 (1996) 3472–3478.
[27] D.C. Clary, J. Phys. Chem. 92 (1988) 3173–3181.
[28] E. Fermi, E. Teller, Phys. Rev. 72 (1947) 399–408.
[29] T. Sommerfeld, Phys. Chem. Chem. Phys. 4 (2002) 2511–2516.
[30] G.L. Gutsev, R.J. Bartlett, J. Chem. Phys. 105 (1996) 8785–8792.
[31] R.F.M. Lobo, A.M.C. Moutinho, K. Lacmann, J. Los, J. Chem. Phys. 95 (1991) 166–175.
[32] I.C. Walker, M.A.D. Fluendy, Int. J. Mass Spectrom. 205 (2001) 171–182.
[33] A. Kuhn, H.P. Fenzlaff, E. Illenberger, J. Chem. Phys. 88 (1988) 7453–7458.
[34] M. Orzol, I. Martin, J. Kocisek, I. Dabkowska, J. Langer, E. Illenberger, Phys. Chem. Chem. Phys. 9 (2007) 3424–3431.
[35] L.V. Trepka, H. Neuert, Z. Naturforsch. Pt. A A18 (1963) 1295.
[36] M.G. Curtis, I.C. Walker, J. Chem. Soc. Faraday Trans. 88 (1992) 2805–2810.
[37] Y. Itikawa, N. Mason, J. Phys. Chem. Ref. Data 34 (2005) 1–22.
[38] J. Fedor, P. Cicman, B. Coupier, S. Feil, M. Winkler, K. Gluch, J. Husarik, D. Jaksch, B. Farizon, N.J. Mason, P. Scheier, T.D. Mark, J. Phys. B-At. Mol. Opt. 39 (2006) 3935–3944.
[39] L. Sanche, G.J. Schulz, Phys. Rev. A 6 (1972) 69.
[40] S. Pilling, H.M. Boechat-Roberty, A.C.F. Santos, G.G.B. de Souza, J. Electron Spectrosc. 155 (2007) 70–76.

[41] J. Berkowitz, G.B. Ellison, D. Gutman, J. Phys. Chem. 98 (1994) 2744–2765.
[42] P. Warneck, Z. Naturforsch. Pt. A A26 (1971) 2047.
[43] L. Friedman, F.A. Long, M. Wolfsberg, J. Chem. Phys. 27 (1957) 613–622.
[44] H.S. Kilic, K.W.D. Ledingham, C. Kosmidis, T. McCanny, R.P. Singhal, S.L. Wang, D.J. Smith, A.J. Langley, W. Shaikh, J. Phys. Chem. A 101 (1997) 817–823.
[45] C. Lifshitz, M. Rejwan, I. Levin, T. Peres, Int. J. Mass Spectrom. Ion Process. 84 (1988) 271–282.
[46] R.J. Kandel, J. Chem. Phys. 23 (1955) 84–87.
[47] S. Tsuda, C.E. Melton, W.H. Hamill, J. Chem. Phys. 41 (1964) 689.
[48] B. Ruscic, J. Berkowitz, J. Chem. Phys. 101 (1994) 10936–10946.
[49] J.L. Holmes, J.K. Terlouw, F.P. Lossing, J. Phys. Chem. 80 (1976) 2860–2862.
[50] R.D. Bowen, A. Maccoll, Org. Mass Spectrom. 19 (1984) 379–384.
[51] K.M.A. Refaey, W.A. Chupka, J. Chem. Phys. 48 (1968) 5205.
[52] Y. Niwa, T. Nishimura, H. Nozoye, T. Tsuchiya, Int. J. Mass Spectrom. Ion Process. 30 (1979) 63–73.
[53] M.A. Haney, J.L. Franklin, J. Chem. Phys. 50 (1969) 2028.
[54] A.N. Stepanov, A.A. Perov, S.P. Kabanov, A.P. Simonov, High. Energ. Chem. 22 (1988) 81–85.
[55] V.H. Dibeler, J.A. Walker, H.M. Rosenstock, J. Res. Natl. Bureau Stand.-A: Phys. Chem. 70 (1966) 459–463.